Supporting Information

Regulating Multiple Self-Trapped Exciton Emissions in Zero-Dimensional Antimony Halide with Pyramidal Units

Jiang Han, [a] *Qian Li,* [*b] *Bin Xu,* [a] *Li Tan,* [a] *Yulin Chen,* [a] *and Zewei Quan* [*a]

[a] Department of Chemistry, Southern University of Science and Technology (SUSTech), Shenzhen, Guangdong 518055, China

[b] Shandong Key Laboratory of Optical Communication Science and Technology, School of Physics Science and Information Technology, Liaocheng University, Liaocheng 252000, China

* Corresponding author

E-mail: quanzw@sustech.edu.cn
liqian@lcu.edu.cn

Experimental section

Chemicals and Materials.

Antimony (III) chloride ($SbCl_3$, 99.95 %) was purchased from Alfa Aesar. Tetraphenylphosphonium chloride ($C_{24}H_{20}PCl$, 98 %) was purchased from Energy Chemical. N, N-dimethylformamide (DMF, ≥99.5 %) was purchased from Shanghai Lingfeng Chemical Reagent). Ethyl acetate (≥99.5 %) was purchased from Xilong Scientific. All reagents and solvents were used without further purification.

Synthesis of $(C_{24}H_{20}P)_2SbCl_5$ single crystal

Briefly, 0.5 mmol $SbCl_3$ and 1.0 mmol $C_{24}H_{20}PCl$ were mixed at the molar ratio of 1:2, and dissolved in 1.5 ml DMF with ultrasonic for 15 min to form the transparent precursor solution. Bulk crystals were obtained by slowly diffusing anti-solvent ethyl acetate into precursor solution at room temperature. The large transparent crystals were collected and dried in vacuum.

Optical characterizations at ambient pressure

The Photoluminescence (PL) and PL excitation (PLE) spectra of $(C_{24}H_{20}P)_2SbCl_5$ were taken by HORIBA Scientific FluoroMax-4 Spectrofluorometer. Time-resolved PL (TRPL) decay spectra of $(C_{24}H_{20}P)_2SbCl_5$ measurements were conducted on an Edinburgh FLS1000 fluorescence spectrometer.

Pressure generation

The high-pressure environment was provided by symmetrical diamond anvil cells (DAC). The type-IIa diamond (400 μm culet size in diameter) was utilized to conduct high-pressure experiments. The sample chambers were 150 μm diameter holes, drilled in the center of the pre-indented T301 steel gaskets. Silicon oil was employed as pressure-transmitting medium for all the experiments. The pressure value was calibrated using the ruby fluorescence technique.[1]

High-pressure characterizations

The high-pressure PL emission of $(C_{24}H_{20}P)_2SbCl_5$ was detected by the NOVA spectrometer with the laser excitations at 3.82 eV (325 nm). The PL micrographs were captured with the same exposure time for the same run of high-pressure experiment, using the CCD camera equipped on the microscope. For the combined high-pressure experiments at low temperature, the DAC was placed in the cryogenic vacuum chamber and clamped to the cold-finger of the liquid nitrogen flow cryostat (ST-500 from Janis). The UV-Vis absorption spectra upon pressure were collected by the fiber spectrometer of Ocean Optics QE6500 with deuterium-

halogen light source. The bandgap measured by absorption method is determined by extrapolating the linear portion of the α^2 versus the hν curve, where α is the absorption coefficient, h is Planck constant, and ν is the frequency of the photon. High-pressure Raman spectra were collected under a 2.33 eV (532 nm) excitation with HORIBA iHR550 spectrometer. High-pressure angle-dispersive X-ray diffraction (ADXRD) experiments were performed at beamline 4W2, Beijing Synchrotron Radiation Facility (BSRF). The ambient CeO_2 powder was applied to calibrate the parameters of detector. The wavelength of incident X-ray beam is 0.6199 Å. The one-dimensional ADXRD spectra were obtained by integrating two-dimensional images using the Dioptas program.[2]

Data analyses

The Arrhenius plot of integrated PL intensity *vs* inverse temperature is fitted by the following equation:

$$I(T) = \frac{I_0}{1+C_1 exp(\frac{-E_a}{kT})}$$

where I_0 and C_1 are constants, and E_a activation energies. The fitted values of I_0, C_1 are 0.9, 9.1×10^6, respectively, and E_a is 145.3 meV indicating a strong nonradiative transition above 168 K. [3]

To evaluate Huang−Rhys factors (*S*) of different triplet states in $(C_{24}H_{20}P)_2SbCl_5$, the temperature-dependent full width at half maxima (FWHM) is modeled using the theory of Toyozawa:

$$\mathrm{FWHM} = 2.36\sqrt{S}\hbar\omega\sqrt{\coth(\frac{\hbar\omega}{2k_BT})}$$

Here *S* is the Huang−Rhys factor, $\hbar$ is the reduced Planck constant, ω is the phonon frequency, k_B is the Boltzmann constant, and T temperature. [4, 5]

Pawley refinements were conducted using the Materials Studio program with reflex module.

The pressure-volume (P-V) data fitting was performed based on the third-order Birch−Murnaghan equation of state as follows:

$$P(V) = \frac{3}{2}B_0\left[\left(\frac{V_0}{V}\right)^{\frac{7}{3}} - \left(\frac{V_0}{V}\right)^{\frac{5}{3}}\right]\left\{1+\frac{3}{4}(B_0'-4)\left[\left(\frac{V_0}{V}\right)^{\frac{2}{3}}-1\right]\right\}$$

where B_0 represents the ambient bulk modulus, B_0' is the pressure derivative of the bulk modulus, V_0 is the lattice volume as zero pressure.

To evaluate the distortions of $[SbCl_5]^{2-}$ pyramid, the five-coordinate pyramidal parameters of δ^2 and λ were calculated with the following equations:

$$\delta^2 = \frac{1}{7}\sum_{i=1}^{8}(\theta_i - 90^{\circ})^2$$

$$\lambda = \frac{1}{5}\sum_{i=1}^{5}\left(\frac{d_i - d_0}{d_0}\right)^2$$

In these equations, the θ_i is the bond angles in $[SbCl_5]^{2-}$ pyramid, and d_0 is the average bond angle of the $[SbCl_5]^{2-}$ pyramid.[6, 7] The parameters of d_i and d_0 represent the individual bond distance and average bond distance of Sb-Cl within the $[SbCl_5]^{2-}$ pyramid, respectively.

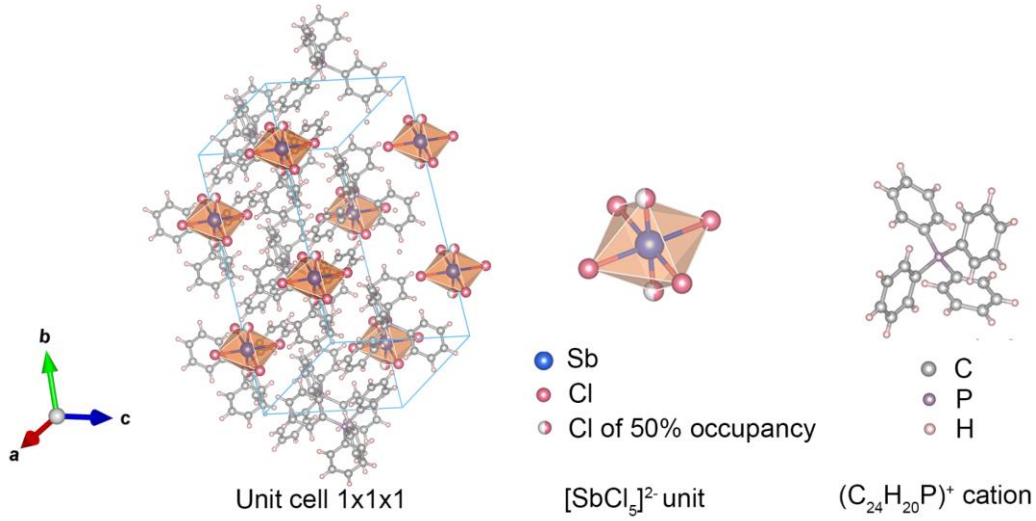

Figure S1. The crystal structure of $(C_{24}H_{20}P)_2SbCl_5$ at ambient conditions. Sb, Cl, C, H and P atoms are illustrated with different colors of blue, light red, grey, pink, and purple, respectively. Mixed color represents Cl atoms of 50% atomic occupancy.

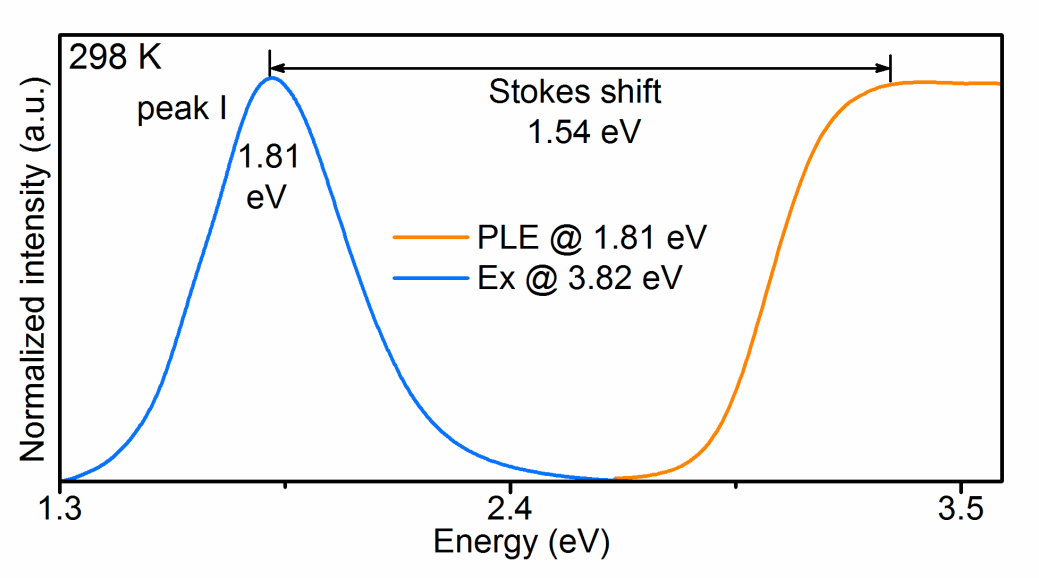

Figure S2. The PL (excitation at 3.82 eV, 325 nm) and PLE (emission at 1.81 eV, 685 nm) spectra of $(C_{24}H_{20}P)_2SbCl_5$ at ambient conditions. Ex is short for excitation.

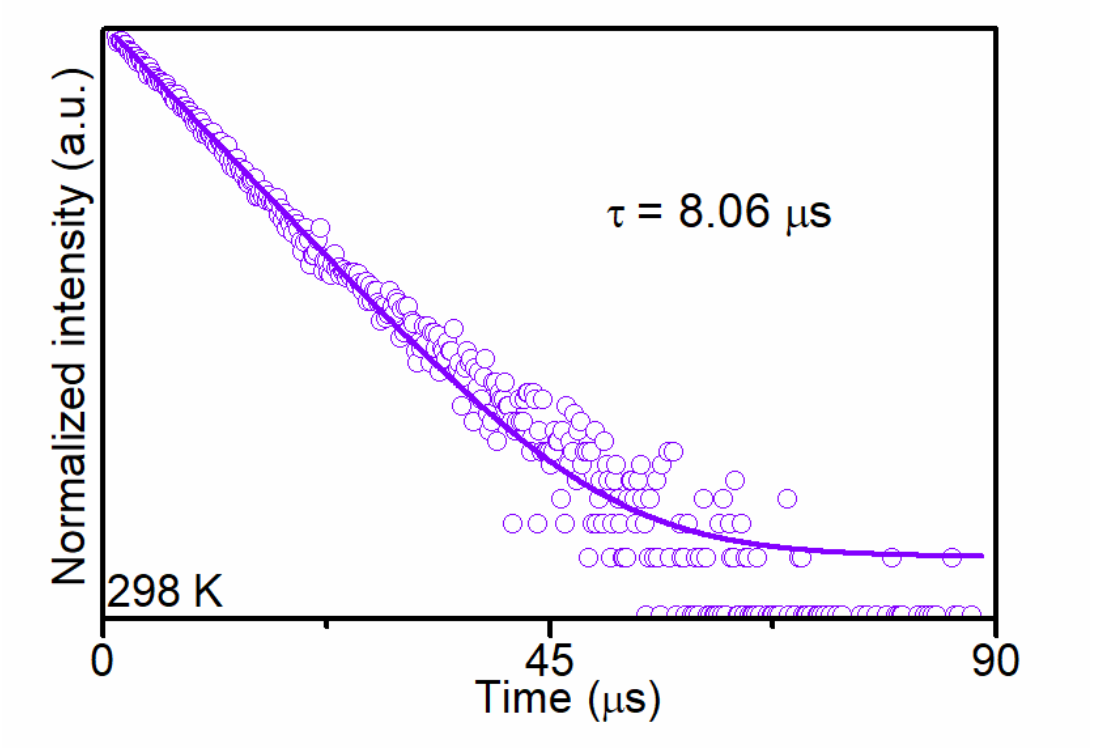

Figure S3. The time-resolved PL decay curve of $(C_{24}H_{20}P)_2SbCl_5$ at ambient conditions. The lifetime is measured under the excitation at 4.00 eV (310 nm).

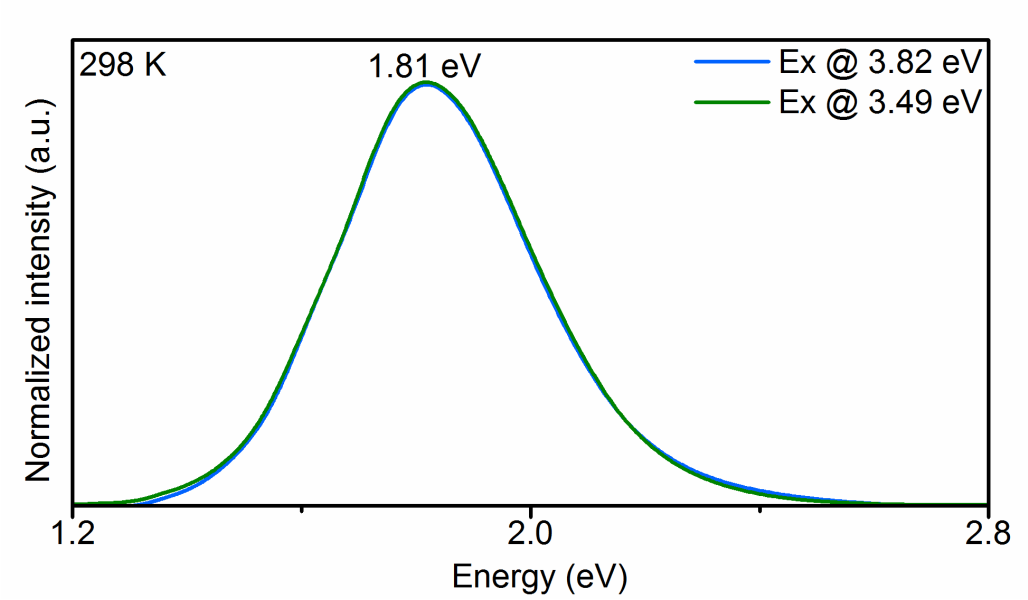

Figure S4. The ambient PL spectra of $(C_{24}H_{20}P)_2SbCl_5$ under the different excitations at 3.82 eV (325 nm) and 3.49 eV (355 nm).

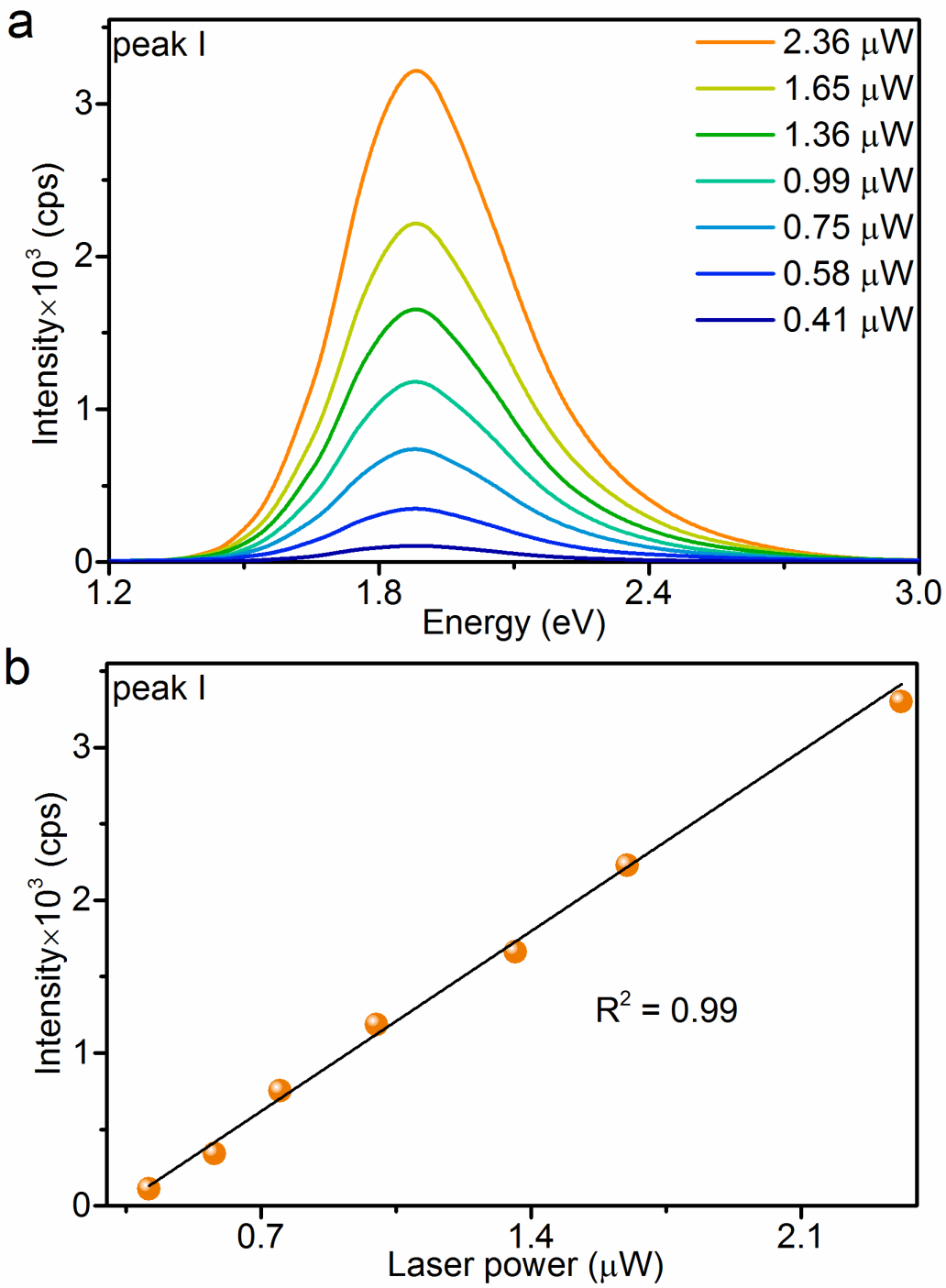

Figure S5. (a) The power-dependent PL spectra of $(C_{24}H_{20}P)_2SbCl_5$ at ambient conditions. The PL signals are detected under excitation at 3.82 eV (325 nm). (b) The linear fit of the corresponding intensity-power data.

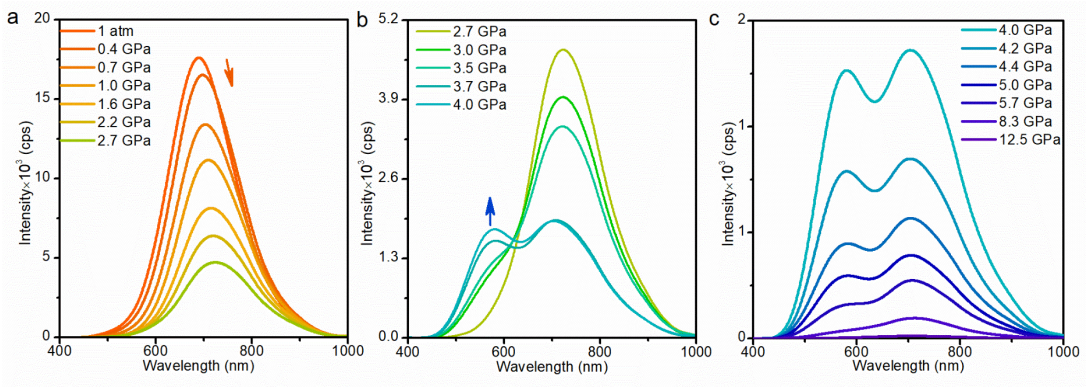

Figure S6. Pressure-dependent PL emission of $(C_{24}H_{20}P)_2SbCl_5$ at room temperature.

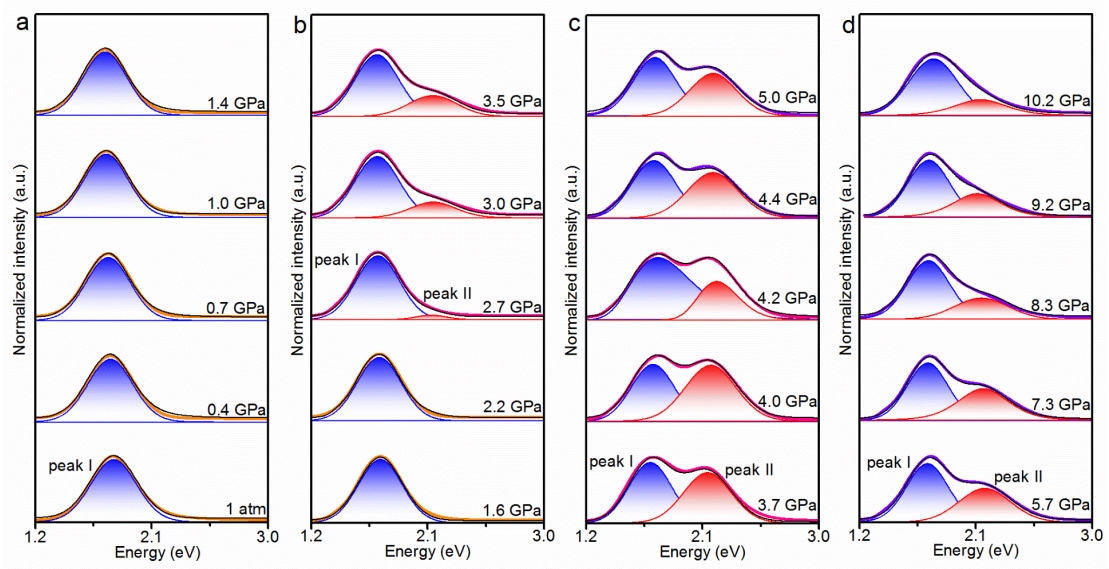

Figure S7. High-pressure PL emission of $(C_{24}H_{20}P)_2SbCl_5$ at room temperature. The fitted peak I and peak II are illustrated with different colors of blue and red, respectively.

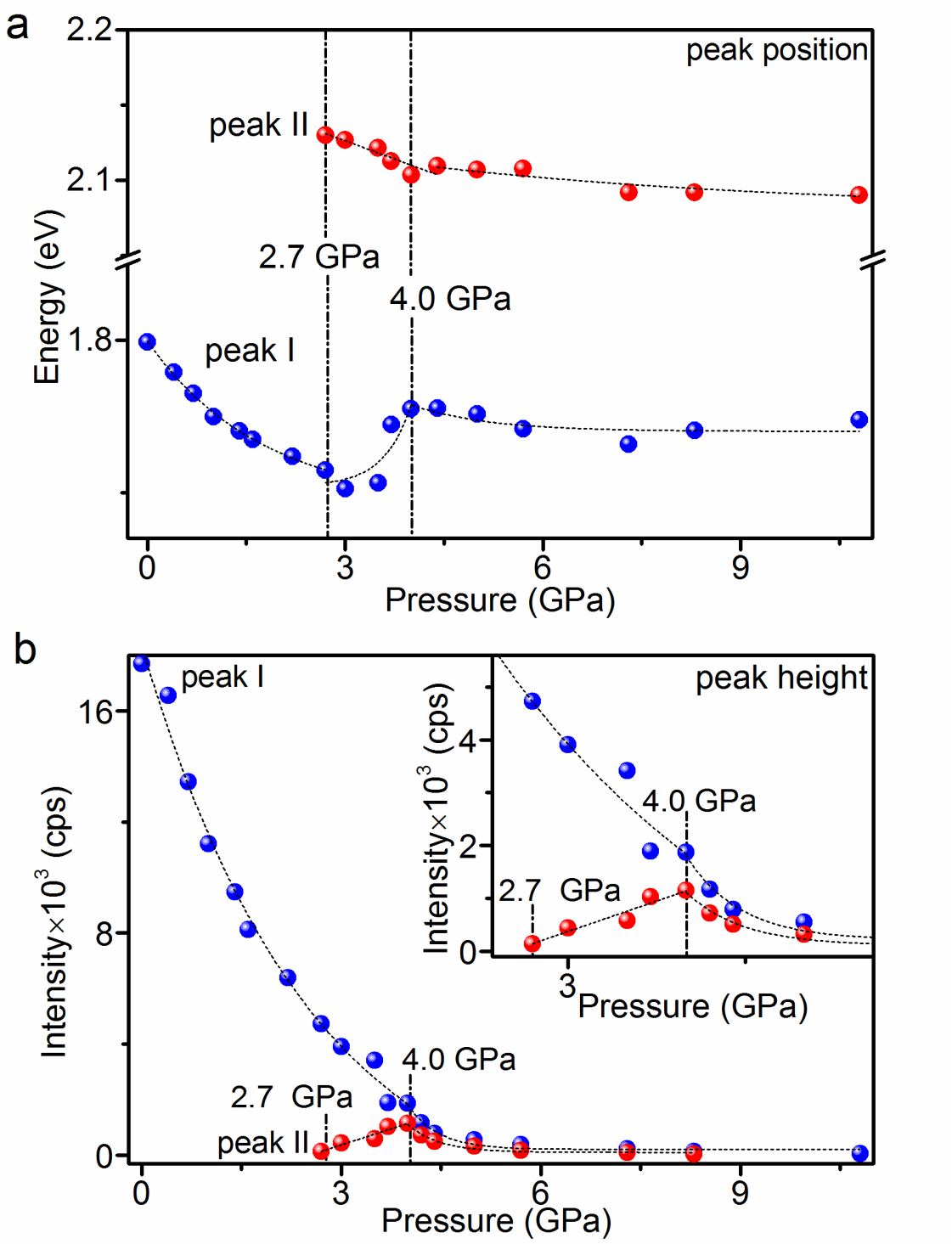

Figure S8. High-pressure evolutions of (a) peak positions and (b) peak heights during compression. The data of peak I and peak II is illustrated with different colors of blue and red, respectively.

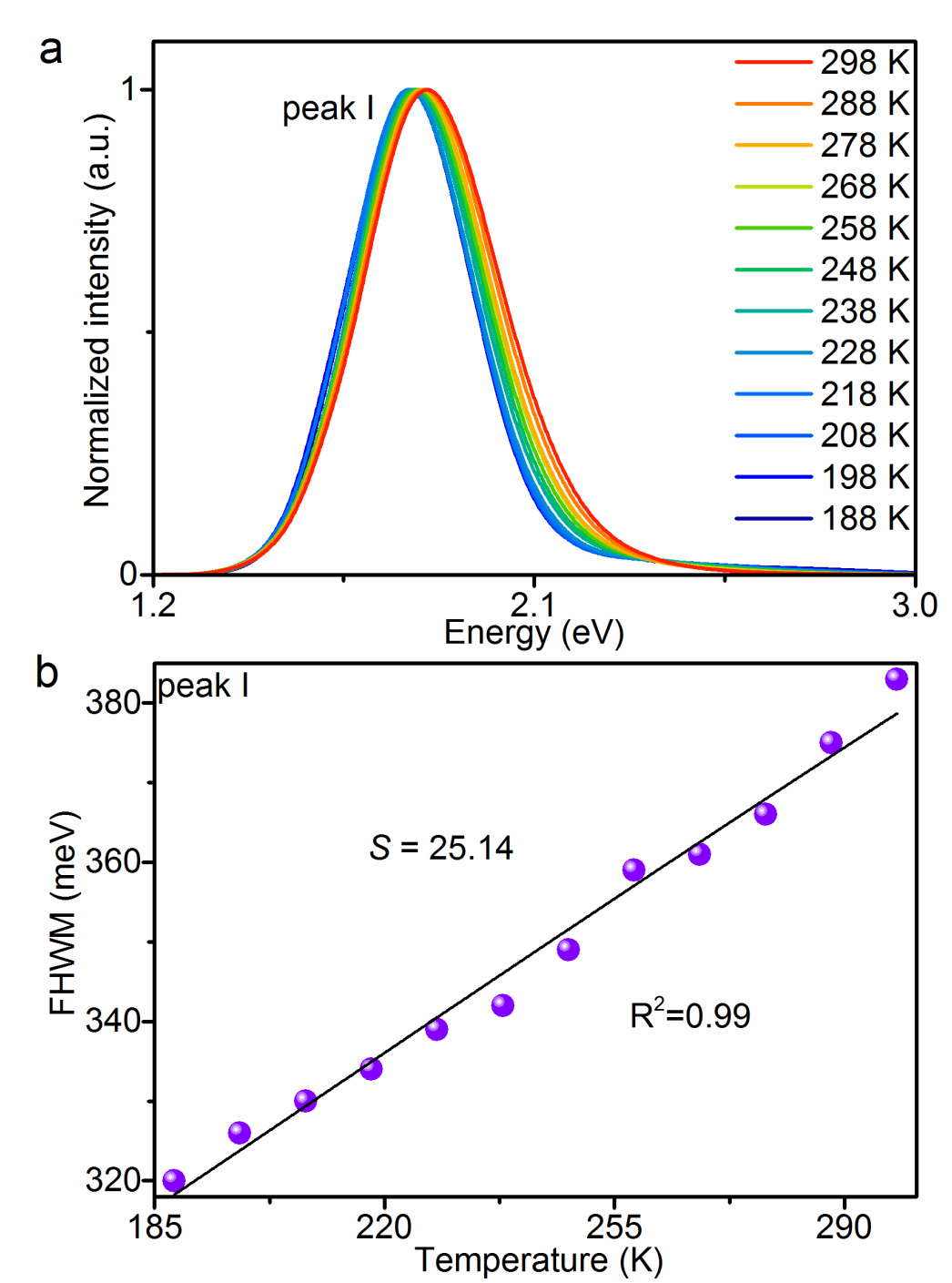

Figure S9. (a) The temperature-dependent PL spectra of peak I. (under excitation at 3.82 eV, 325 nm). (b)The evolution of FWHM as function of temperature. The calculation of Huang-Rhys (*S*) factor is based on the theory of Toyozawa.

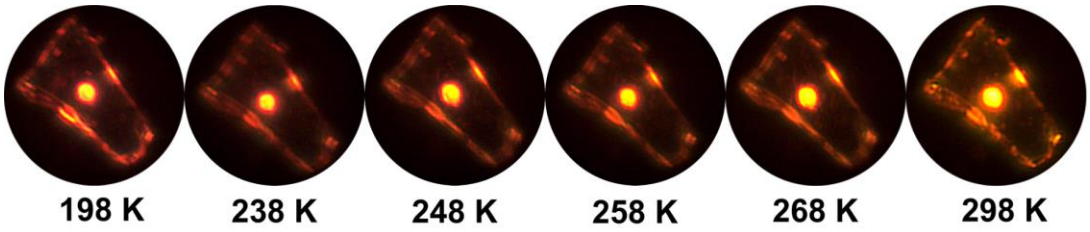

Figure S10. The PL images of $(C_{24}H_{20}P)_2SbCl_5$ crystal upon cooling from 298 K to 198K. The images are captured under excitation at 3.82 eV (325 nm).

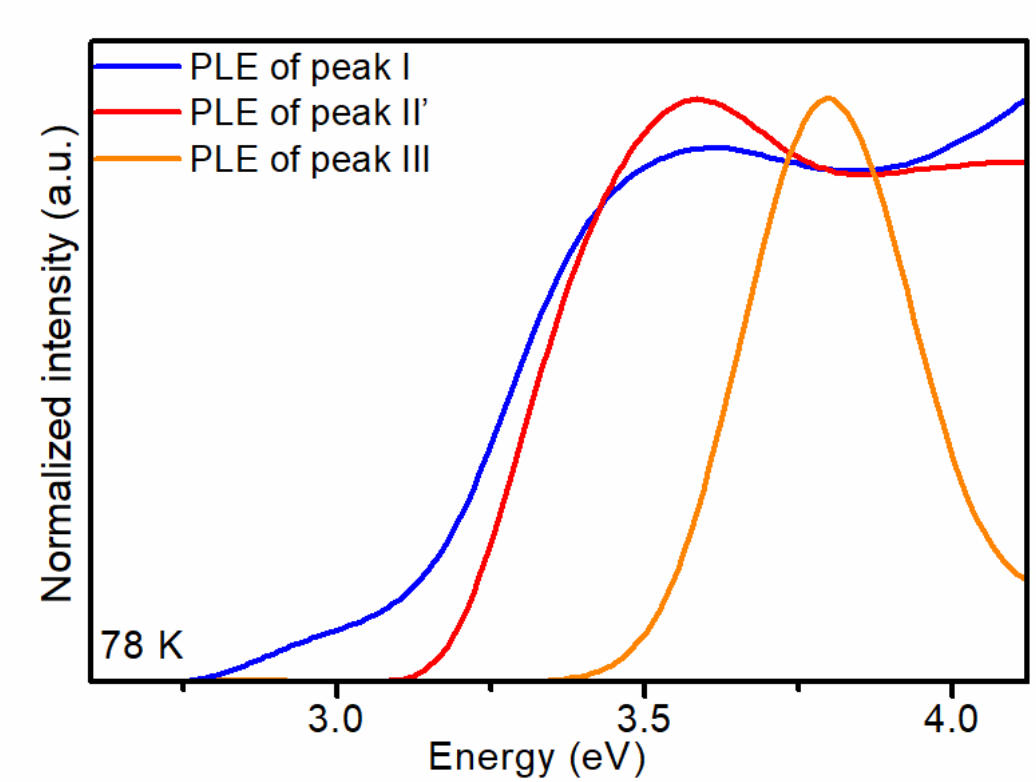

Figure S11. The PLE spectra of peak I (emission at 1.81 eV), peak II' (emission at 2.12 eV) and peak III (emission at 2.43 eV) at 78 K. The PLE spectra of peak I, peak II' and peak III are illustrated with different colors of blue, red and orange, respectively.

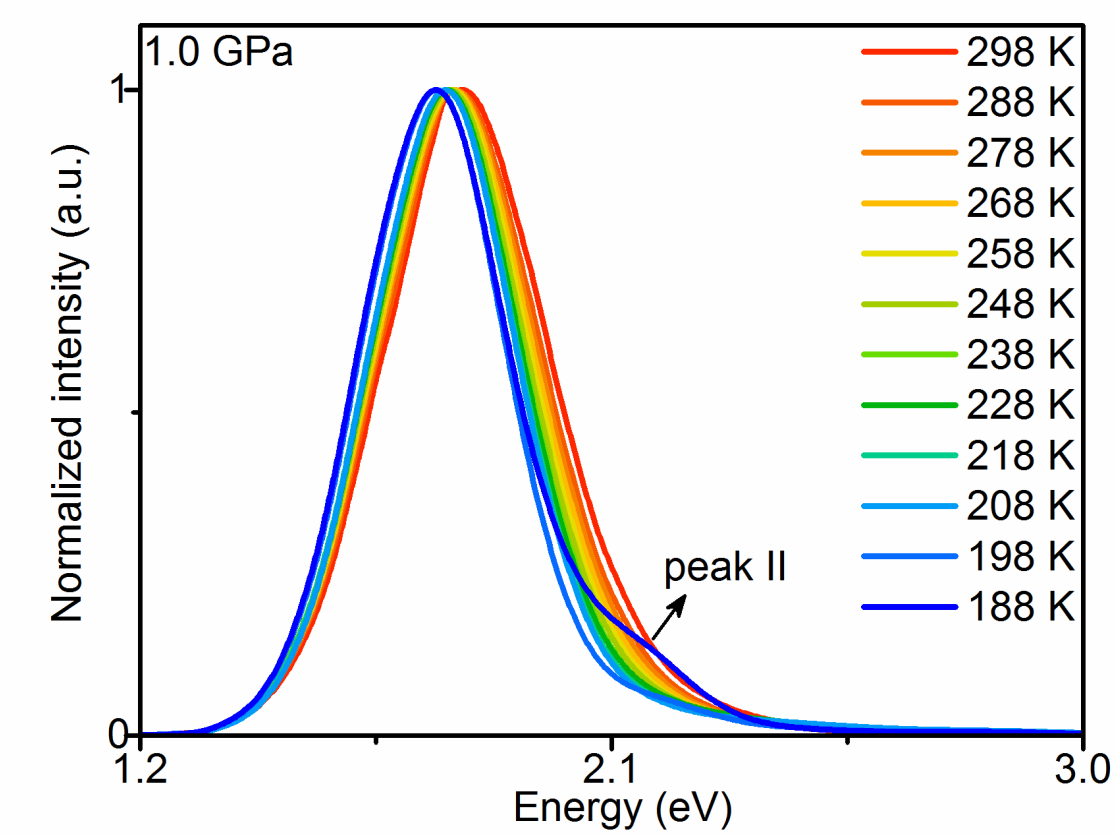

Figure S12. The temperature-dependent PL spectra of $(C_{24}H_{20}P)_2SbCl_5$ at 1.0 GPa under 3.82 eV (325 nm) excitation.

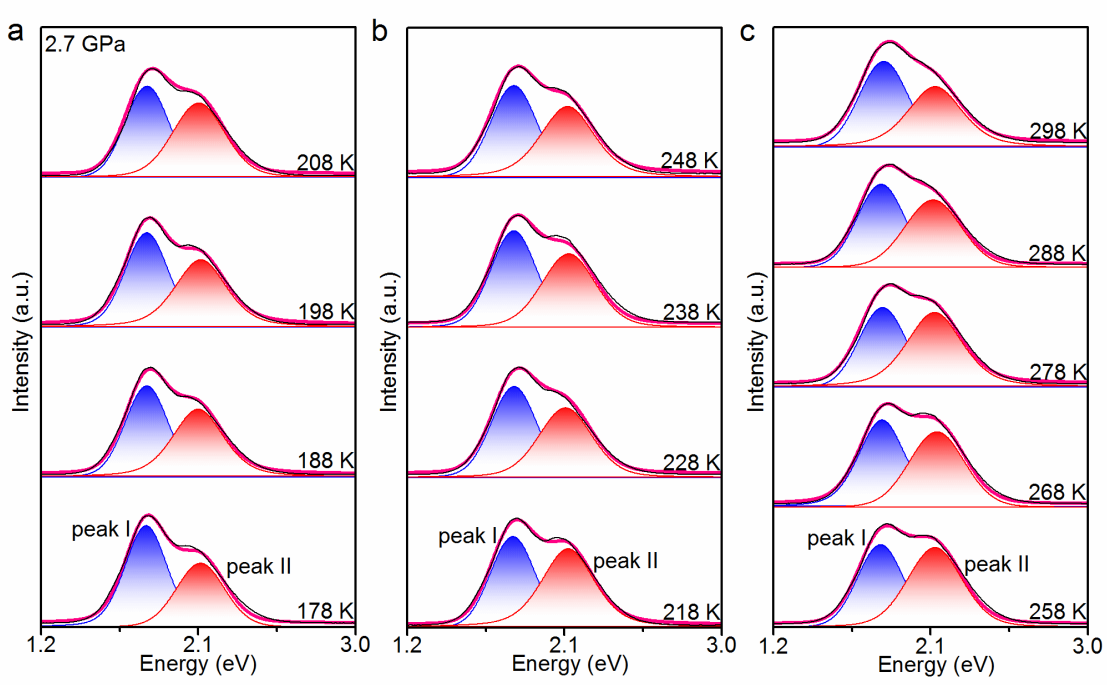

Figure S13. The temperature-dependent PL spectra of $(C_{24}H_{20}P)_2SbCl_5$ at 2.7 GPa. The PL spectra are detected under 3.82 eV (325 nm) excitation. The fitted peak I and peak II are illustrated with different colors of blue and red, respectively.

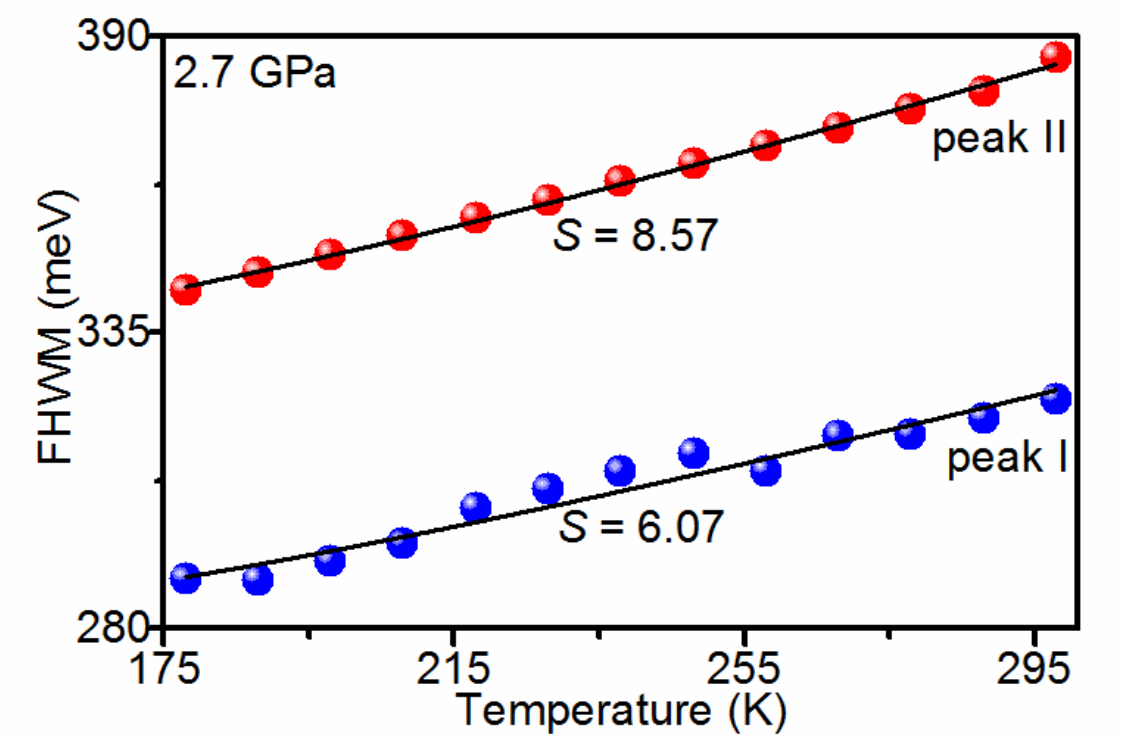

Figure S14. The temperature-dependent FWHM of PL emission of $(C_{24}H_{20}P)_2SbCl_5$ at 2.7 GPa. The *S* factor is calculated based on the theory of Toyozawa. The data of peak I and peak II is illustrated with different colors of blue and red, respectively.

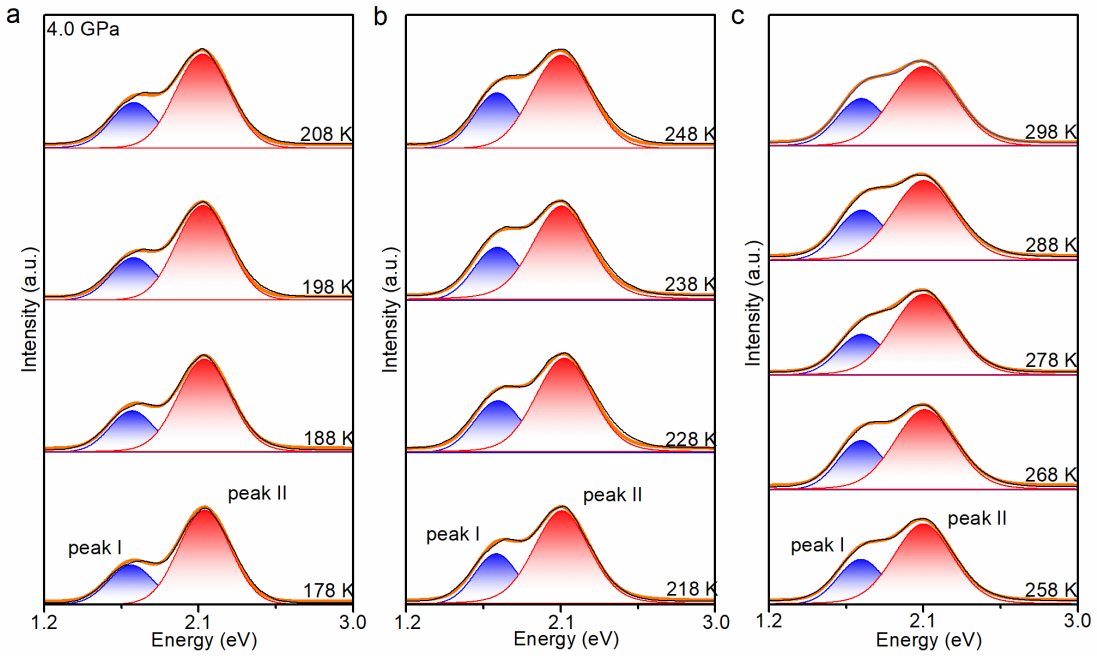

Figure S15. The temperature-dependent PL spectra of $(C_{24}H_{20}P)_2SbCl_5$ at 4.0 GPa. The PL spectra are detected under 3.82 eV (325 nm) excitation. The fitted peak I and peak II are illustrated with different colors of blue and red, respectively.

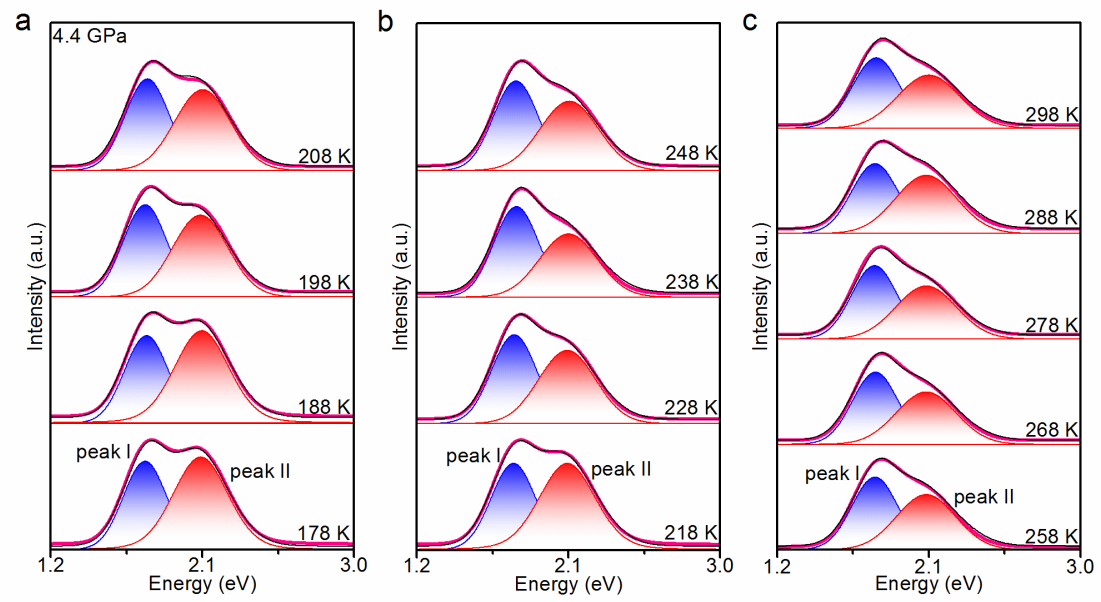

Figure S16. The temperature-dependent PL spectra of $(C_{24}H_{20}P)_2SbCl_5$ at 4.4 GPa. The PL emission are detected under 3.82 eV (325 nm) excitation. The fitted peak I and peak II are illustrated with different colors of blue and red, respectively.

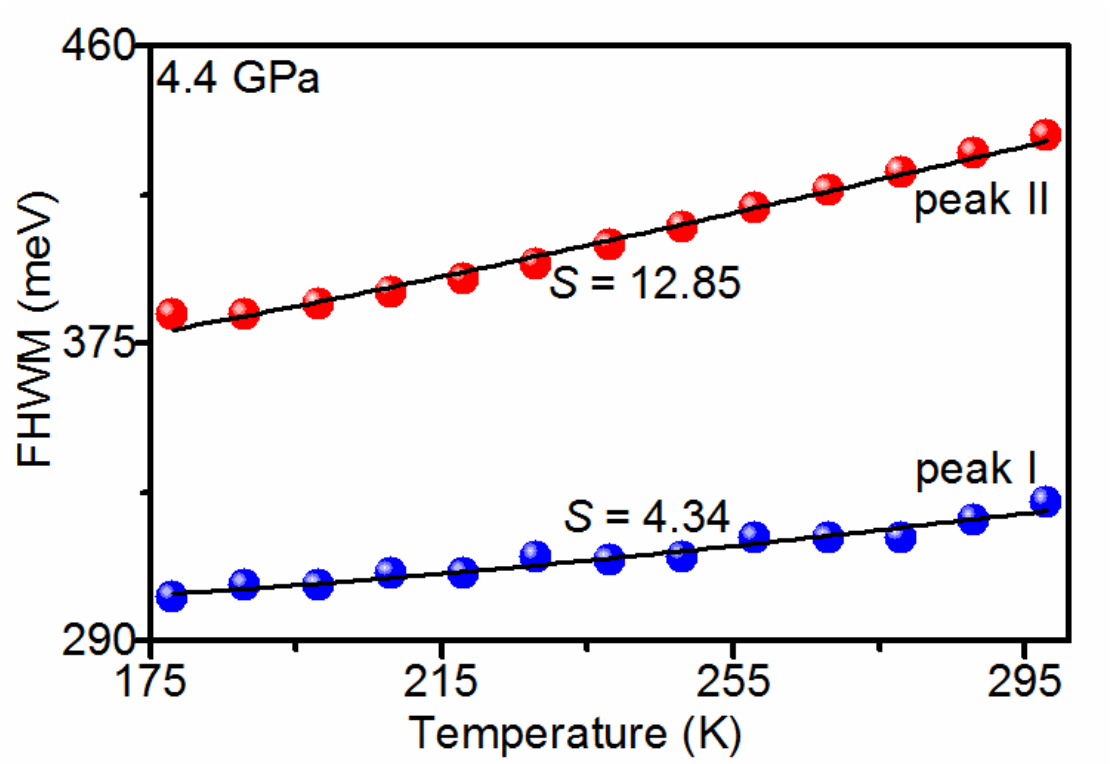

Figure S17. The temperature-dependent FWHM of PL emission of $(C_{24}H_{20}P)_2SbCl_5$ at 4.4 GPa. The *S* factor is calculated using the theory of Toyozawa. The data of peak I and peak II is illustrated with different colors of blue and red, respectively.

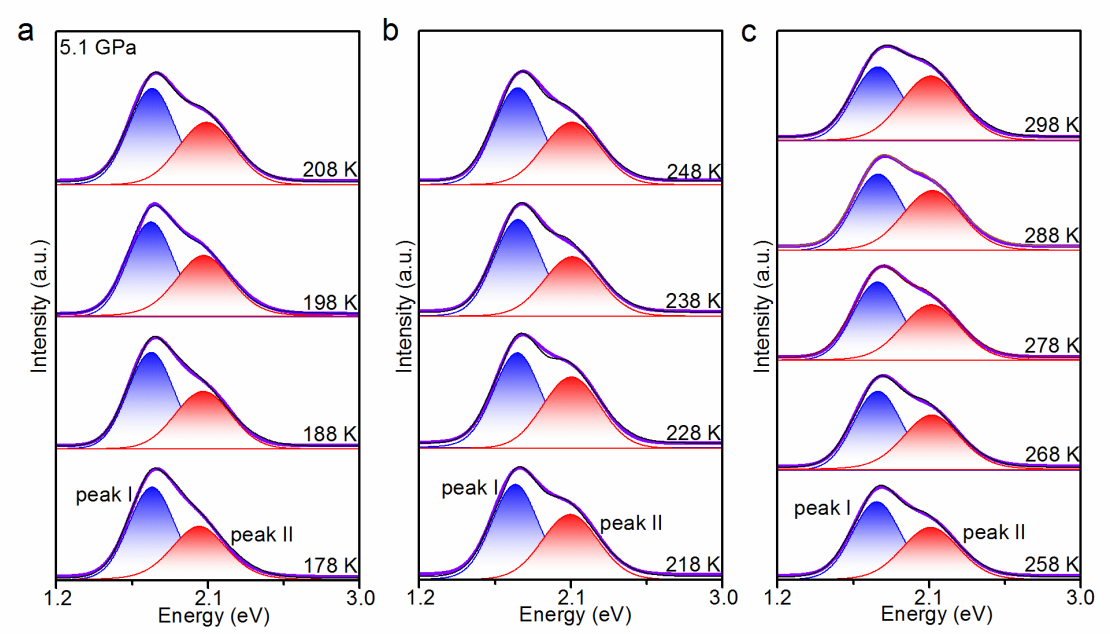

Figure S18. The temperature-dependent PL spectra of $(C_{24}H_{20}P)_2SbCl_5$ at 5.1 GPa. The PL spectra are detected under excitation at 3.82 eV (325 nm). The fitted peak I and peak II are illustrated with different colors of blue and red, respectively.

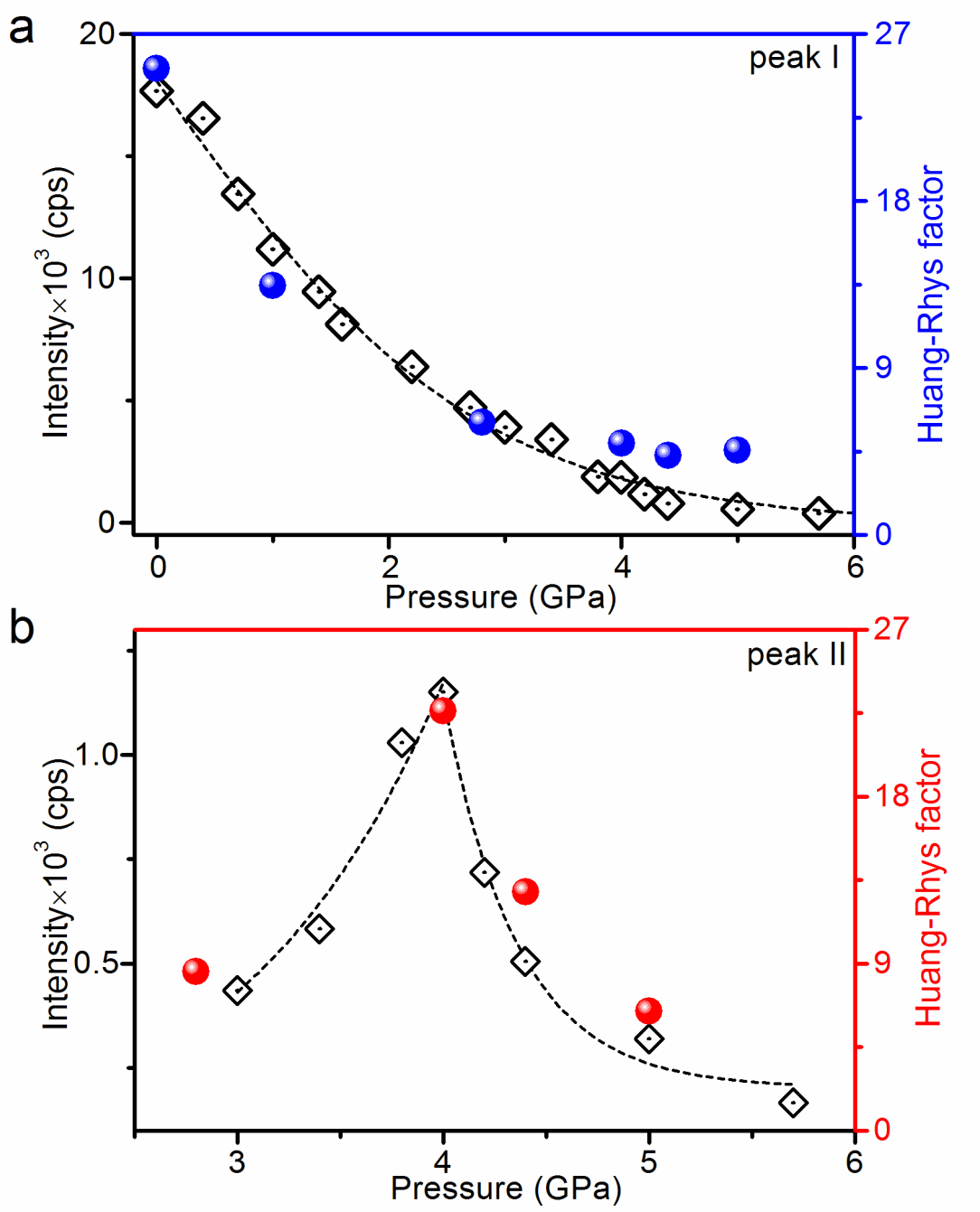

Figure S19. High-pressure evolutions of PL intensities and *S* factors of peak I (a) and peak II (b).

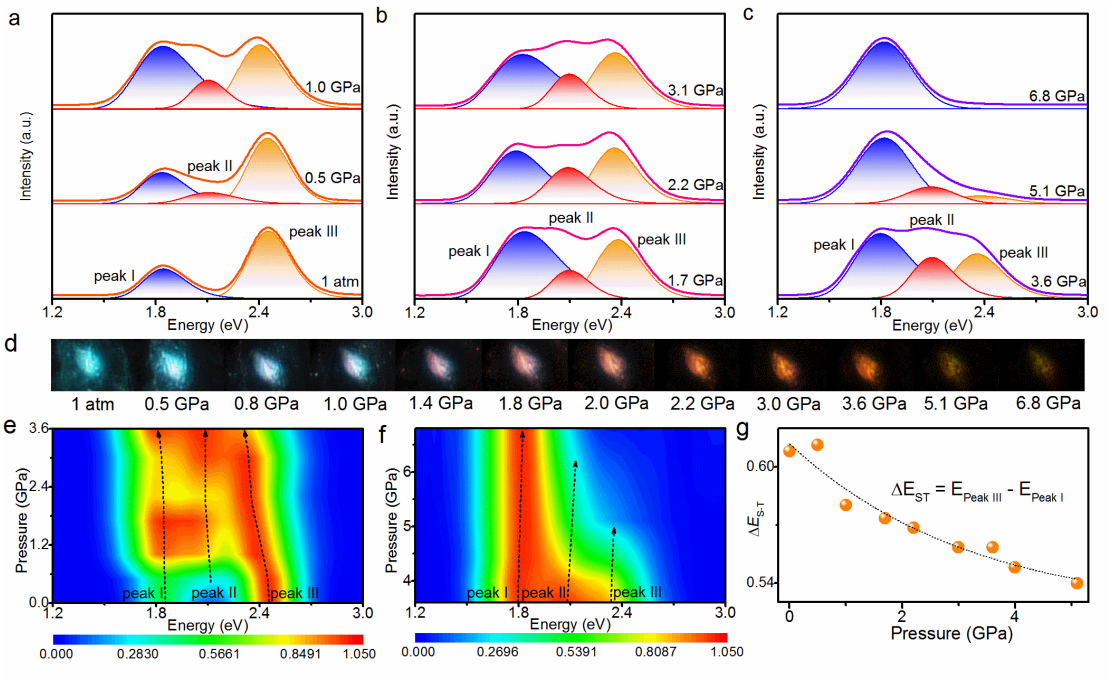

Figure S20. (a-c) The PL spectra of $(C_{24}H_{20}P)_2SbCl_5$ at 78 K upon compression from 1 atm to 6.8 GPa. (d) Pressure-dependent PL images of 78 K. The images are captured under the laser excitation at 3.82 eV (325 nm). (e-f) Two-dimensional projection of emission intensities upon pressure from 1 atm to 6.8 GPa. (g) High-pressure evolution of the energy difference ΔE_{ST} between triplet peak I and singlet peak III at 78 K.

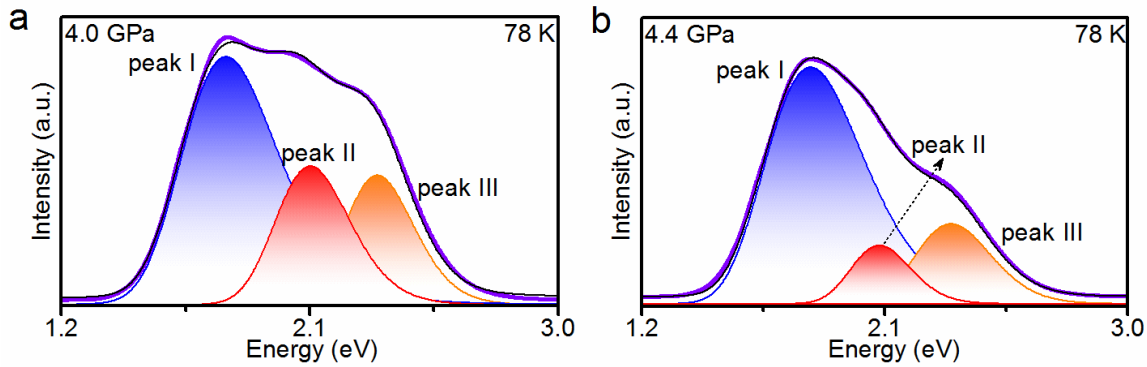

Figure S21. The fitted PL spectra at (a) 4.0 GPa and (b) 4.4 GPa at 78 K. The fitted peak I, peak II and peak III are illustrated with different colors of blue, red and orange, respectively.

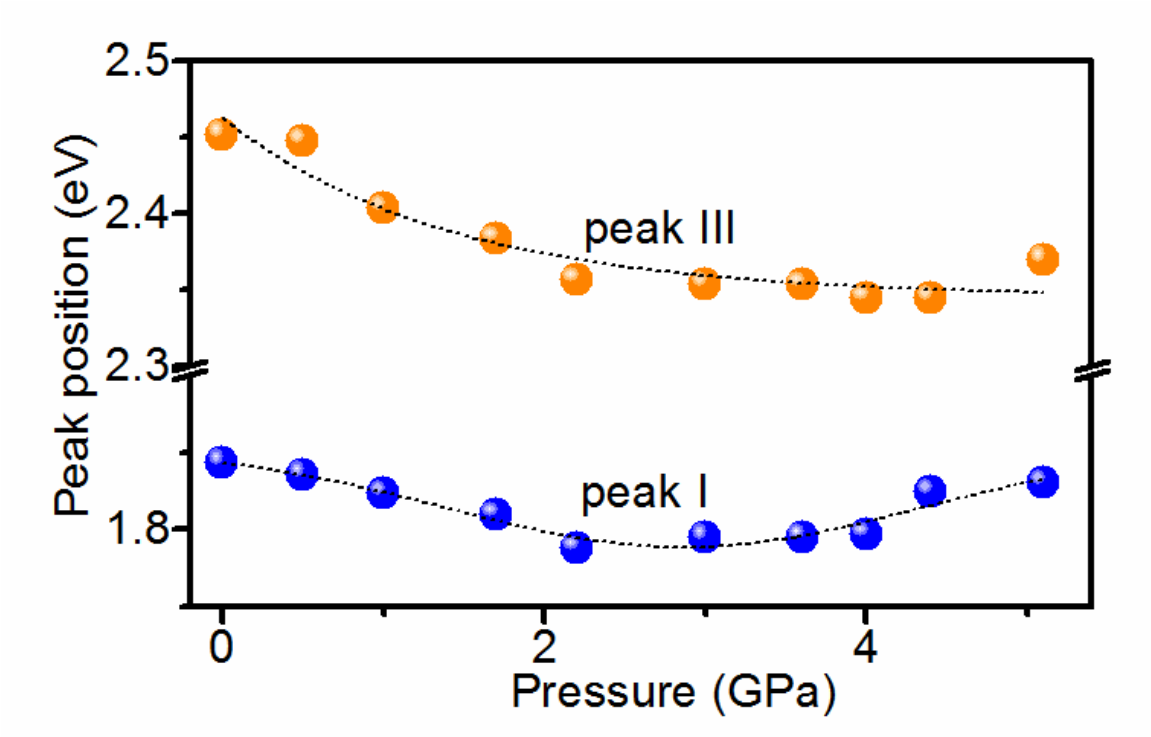

Figure S22. Peak positions of peak I and peak III upon compression.

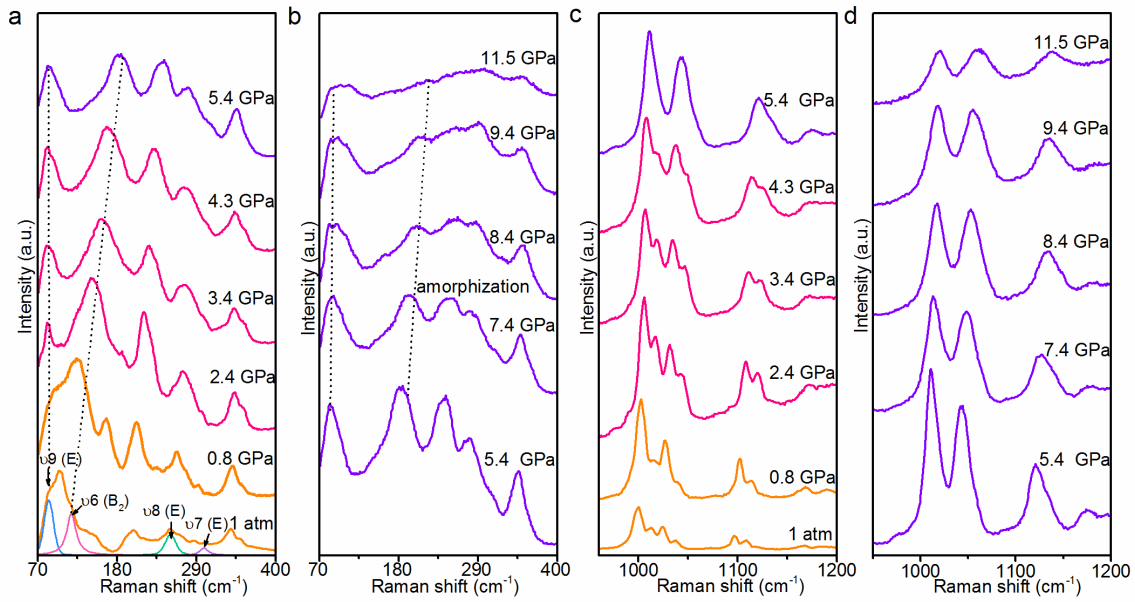

Figure S23. Raman spectra of $(C_{24}H_{20}P)_2SbCl_5$ with increasing pressure. The Raman vibrations are related to the (a-b) inorganic anions and (c-d) organic cations, respectively. The modes of υ_6 and υ_8 involve with the bending vibrations of $[SbCl_5]^{2-}$, and υ_7 involves with the asymmetry stretching vibrations. The mode of υ_9 is indexed to lattice vibration.[8]

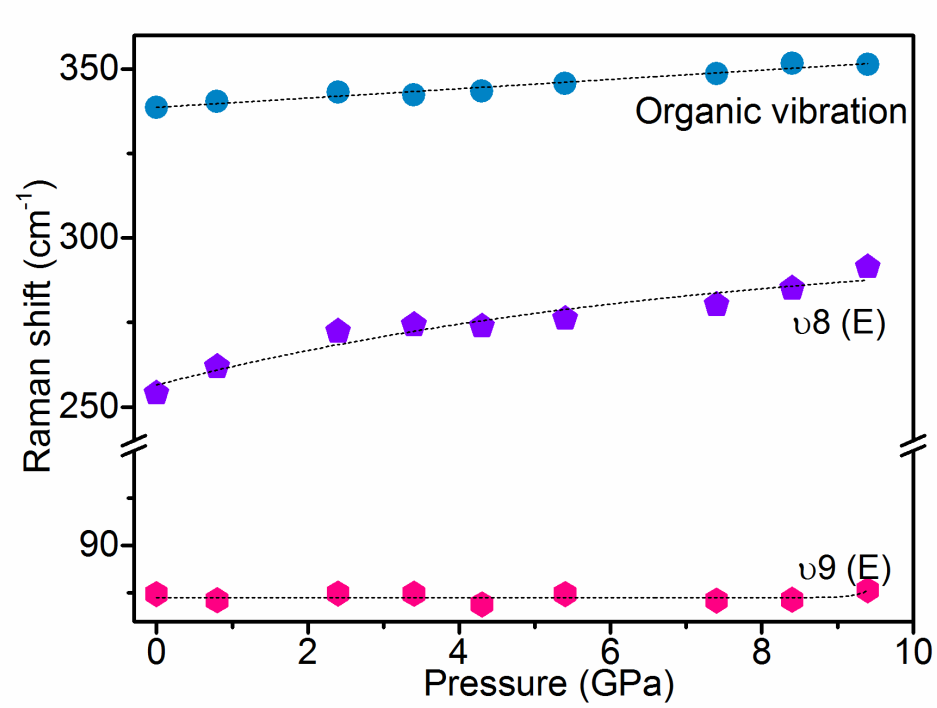

Figure S24. High-pressure evolution of selected vibrations of $(C_{24}H_{20}P)_2SbCl_5$.

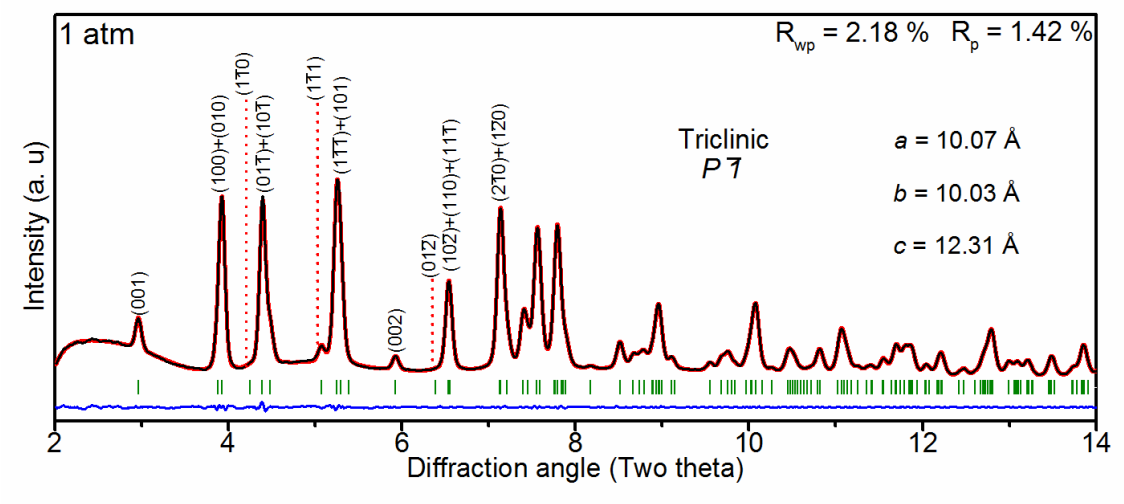

Figure S25. Pawley refinement of ADXRD pattern at ambient conditions (Green bars represent the refined peak positions, and blue line represents the difference between observed (black) and simulated (red) diffraction profiles).

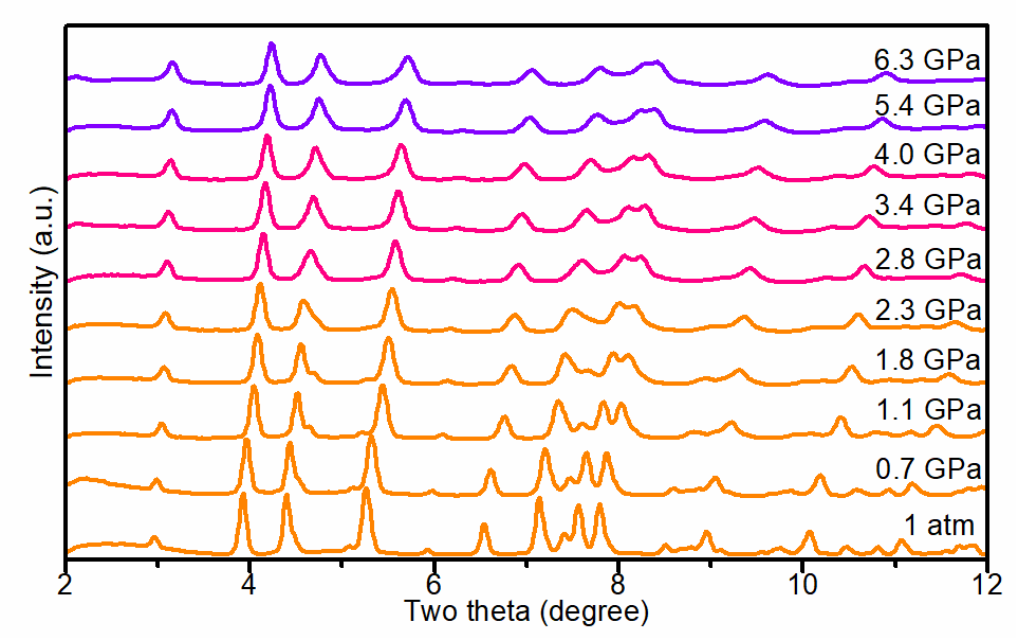

Figure S26. High-pressure structural behaviors of $(C_{24}H_{20}P)_2SbCl_5$.

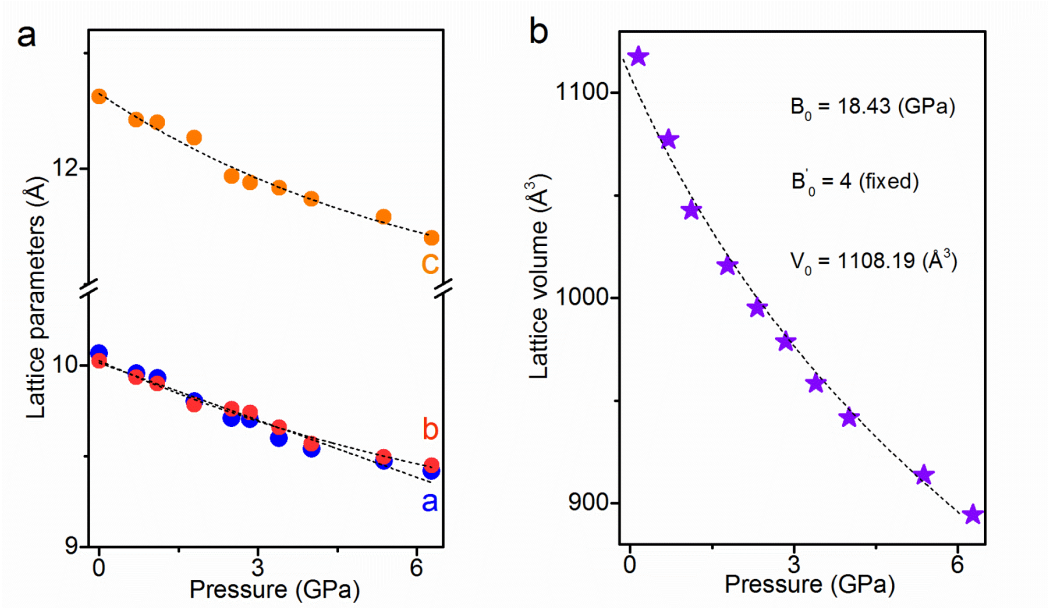

Figure S27. High-pressure evolution of (a) lattice parameters and (b) lattice volume.

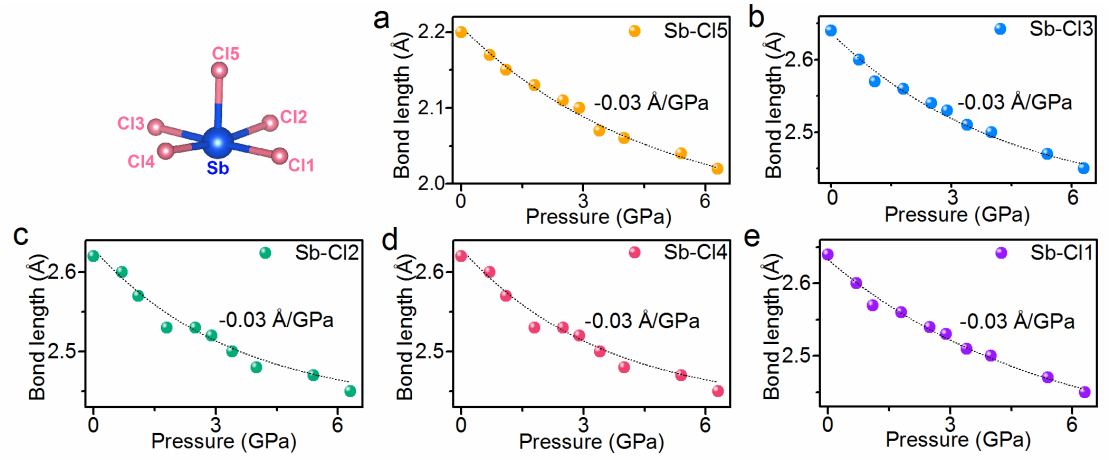

Figure S28. (a-e) High-pressure evolution of bond lengths in $[SbCl_5]^{2-}$ (Inset depicts structural diagram of $[SbCl_5]^{2-}$).

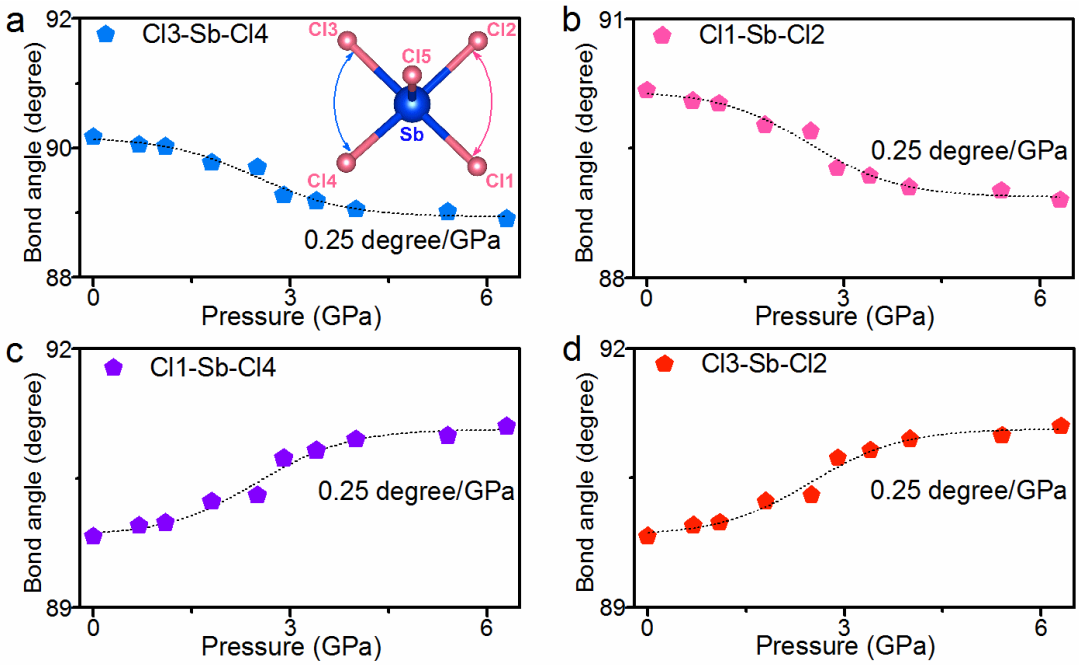

Figure S29. (a-d) High-pressure evolution of bond angles in $[SbCl_5]^{2-}$(Inset depicts bond angles in equatorial plane of $[SbCl_5]^{2-}$).

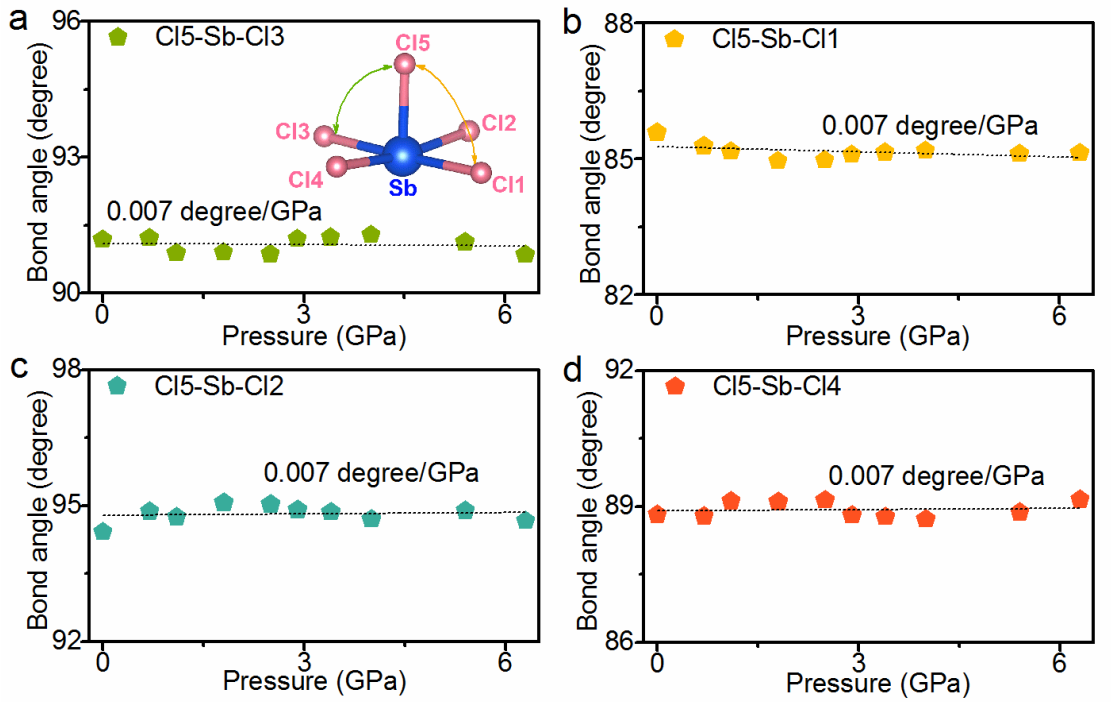

Figure S30. (a-d) High-pressure evolution of bond angles in $[SbCl_5]^{2-}$(Inset depicts bond angles being perpendicular to equatorial plane in $[SbCl_5]^{2-}$).

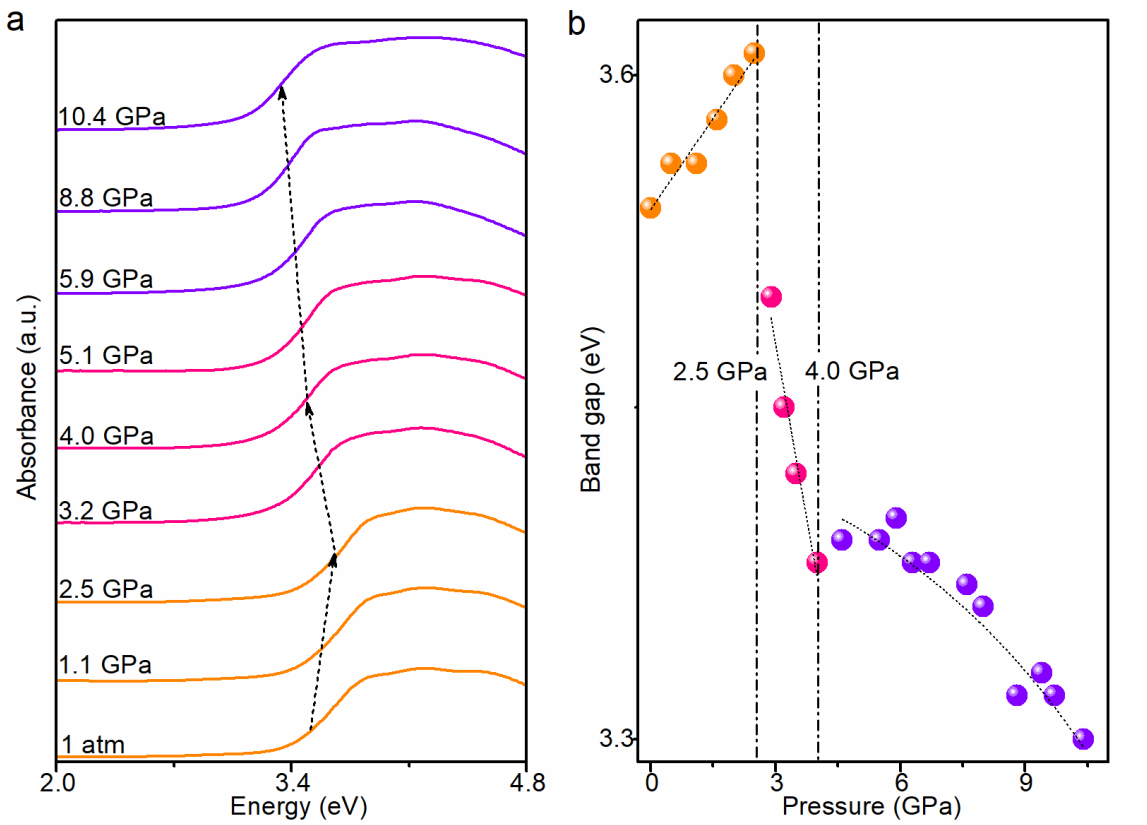

Figure S31. (a) Selected UV-Vis absorption spectra of $(C_{24}H_{20}P)_2SbCl_5$ crystal under compression. (b) Bandgap evolution of $(C_{24}H_{20}P)_2SbCl_5$ as a function of pressure.

Table S1. Ambient bond lengths and deviations λ at 100K and 298 K.

	Sb-Cl5	Sb-Cl3	Sb-Cl2	Sb-Cl1	Sb-Cl4	λ
100 K	2.20	2.62	2.63	2.62	2.63	0.00448
298 K	2.20	2.64	2.62	2.64	2.62	0.00456

Table S2. Ambient bond angles and deviations δ^2 at 100K and 298 K.

	Cl1-Sb-Cl2	Cl1-Sb-Cl4	Cl3-Sb-Cl4	Cl3-Sb-Cl2	Cl5-Sb-Cl1	Cl5-Sb-Cl3	Cl5-Sb-Cl2	Cl5-Sb-Cl4	δ^2
100 K	90.3	90.3	89.7	89.7	85.5	91.2	94.6	90.3	6.17
298 K	90.2	89.8	90.2	89.8	85.6	91.2	94.4	88.8	5.99

References

1. H. K. Mao, P. M. Bell, J. W. Shaner and D. J. Steinberg, Specific volume measurements of Cu, Mo, Pd, and Ag and calibration of the ruby R1 fluorescence pressure gauge from 0.06 to 1 Mbar, *J. Appl. Phys.* 1978, **49**, 3276-3283.
2. C. Prescher and V. B. Prakapenka, DIOPTAS: a program for reduction of two-dimensional X-ray diffraction data and data exploration, *High Pressure Res*, 2015, **35**, 223-230.
3. M. A. Reshchikov and R. Y. Korotkov, Analysis of the temperature and excitation intensity dependencies of photoluminescence in undoped GaN films, *Phys. Rev. B*, 2001, **64**, 115205.
4. Y. Toyozawa, Further Contribution to the Theory of the Line-Shape of the Exciton Absorption Band, *Prog. Theor. Phys*., 1962, **27**, 89-104.
5. W. Stadler, D. M. Hofmann, H. C. Alt, T. Muschik, B. K. Meyer, E. Weigel, G. Müller-Vogt, M. Salk, E. Rupp and K. W. Benz, Optical investigations of defects in $Cd_{1-x}Zn_xTe$, *Phys. Rev. B*, 1995, **51**, 10619-10630.
6. J. Yin, G. Zhang, C. Peng and H. Fei, An ultrastable metal–organic material emits efficient and broadband bluish white-light emission for luminescent thermometers, *Chem. Commun.*, 2019, **55**, 1702-1705.
7. K. Robinson, G. V. Gibbs and P. H. Ribbe, Quadratic Elongation: A Quantitative Measure of Distortion in Coordination Polyhedra, *Science* 1971, **172**, 567-570.
8. H. A. Szymanski, R. Yelin and L. Marabella, Infrared and Raman Spectra of SbCl5=, *J. Chem. Phys* 1967, **47**, 1877-1879.